Quantitative determination of residual silver distribution in nanoporous gold and its influence on structure and catalytic performance

Quantitative Determination of Residual Silver Distribution in Nanoporous Gold and Its Influence on Structure and Catalytic Performance

Christoph Mahr[a,b], Paromita Kundu[c], Anastasia Lackmann[d,b], Daniele Zanaga[c], Karsten Thiel[e], Marco Schowalter[a,b], Martin Schwan[d,b], Sara Bals[c], Arne Wittstock[d,b], Andreas Rosenauer[a,b,*]

[a] *Institute of Solid State Physics, Universität Bremen, Otto-Hahn-Allee 1, 28359 Bremen, Germany*
[b] *MAPEX Center for Materials and Processes, Universität Bremen, Bibliothekstr. 1, 28359 Bremen, Germany*
[c] *EMAT, University of Antwerp, Groenenborgerlaan 171, 2020 Antwerp, Belgium*
[d] *Institute of Applied and Physical Chemistry, Universität Bremen, Leobener Str. UFT, 28359 Bremen, Germany*
[e] *Fraunhofer Institute for Manufacturing Technology and Advanced Materials (IFAM), Wiener Str. 12, 28359 Bremen, Germany*

Abstract

Large efforts have been made trying to understand the origin of the high catalytic activity of dealloyed nanoporous gold as a green catalyst for the selective promotion of chemical reactions at low temperatures. Residual silver, left in the sample after dealloying of a gold-silver alloy, has been shown to have a strong influence on the activity of the catalyst. But the question of how the silver is distributed within the porous structure has not finally been answered yet. We show by quantitative energy dispersive X-ray tomography measurements that silver forms clusters that are distributed irregularly, both on the surface and inside the ligaments building up the porous structure. Furthermore, we find that the role of the residual silver is ambiguous. Whereas CO oxidation is supported by more residual silver, methanol oxidation to methyl formate is hindered. Structural characterisation reveals larger ligaments and pores for decreasing residual silver concentration.

Keywords: nanoporous gold, residual silver, quantitative EDXS tomography, CO oxidation, methanol oxidation, silver cluster

1. Introduction

Nanoporous gold (npAu) has attracted increasing interest over the last years especially because of its high catalytic activity[1–7], its usefulness for sensor or actuator applications[7–9] and its application in fuel cells[10]. Gold (Au) as a catalyst is particularly interesting because of its nontoxic nature, chemical stability and its ability to promote selective reactions at low temperatures[6]. NpAu can be formed either by free or by electrochemical corrosion of a gold master alloy in an acid. During this dealloying process the less noble metal (e.g. silver) is dissolved and a foam like structure built up of ligaments and pores evolves resulting in a porous structure, which is penetrable for gases and liquids[11–13]. The npAu structure is distinguished by a high sur-

*Corresponding author
Email address: rosenauer@ifp.uni-bremen.de (Andreas Rosenauer)

face to volume ratio (specific surface area around $10\,m^2/g$) and a large fraction of low coordinated surface atoms. Although it is disadvantageous in view of the required gold mass, it has advantages as a catalyst in comparison to gold nanoparticles. These are for example a stable structure as sintering is avoided, a tuneable structure from a few nanometres to many microns, and extremely clean surfaces. Similar to Raney Nickel, nanoporous gold is a bulk nanostructured completely unsupported catalyst. Hence, it is also discussed to be a predictable catalyst reflecting the surface chemistry and reactivity of (almost) pure gold[6], in contrast to gold nanoparticles on an oxidic support. However, small fractions of less than 1 at% residual silver (Ag) always remain in the npAu.

Several studies show that bimetallic Au-Ag nanoparticles as powder or supported by an oxide reveal an enhanced catalytic activity by a few orders of magnitude compared to bare Au for oxidation reactions using molecular oxygen (O_2)[14–16]. Also for npAu it has been shown that silver has a strong influence on its catalytic activity[4,6,16,17] as well as on the elastic properties[18]. Haruta concluded in this context that it is likely to address npAu an inversely supported gold catalyst[19]. However, the assets and drawbacks of more or less residual silver are ambiguous[4,6,17] and vary with the nature of the catalytic reaction. Furthermore, besides the fact that the catalytic performance depends on many experimental parameters such as temperature, partial pressures and acidity, the surface chemistry and hence the origin of catalytic activity can also vary depending on whether the reaction takes place in liquid or gaseous environment[20–22]. Therefore, we investigate and compare the catalytic oxidation of CO to CO_2 in gas phase and of methanol to methyl formate in liquid phase as a function of the residual silver concentration.

To understand the role of residual silver in the performance of npAu it is important to know how the silver is spatially distributed within the porous structure. Up to now, there are only limited informations[23] and speculations provided in literature. Different studies show that ligaments with higher silver concentrations are smaller than ligaments with approximately no silver[4,18]. Further, it has been found that short dealloying times result in higher silver concentrations and that the silver concentration is not homogeneous in the nanoporous structure: a higher silver concentration in the center of a cross-section of a npAu disc of $300\,\mu m$ thickness has been found compared to the concentration close to the outer surface of the disc[18]. However, a quantification of the Ag distribution within single ligaments has not been reported so far. Silver concentrations on the surfaces of gold-silver nanoparticles that are different from the average composition have been reported[15] which is also supported by different publications, in which higher metallic silver concentrations on the surface of the nanoporous gold samples compared to the average silver concentration have been found[1,17]. Haruta suggests small Ag_2O particles or patches on the surfaces of the ligaments leading to higher activities compared to the pure npAu catalyst[19]. Theoretical studies show that the presence of low coordinated surface gold atoms is essential, but not sufficient, to explain the high catalytic activity of npAu[24,25], in particular with respect to the activa-

tion of O_2. The authors suggest that chemisorbed CO interacts with atomic oxygen co-adsorbed at nearby Ag atoms. This coincides with the observation that CO prefers adsorption at low coordinated gold sites[14] whereas O_2 highly prefers adsorption on Ag[15]. In this manner, catalytic activity for CO oxidation can be enhanced by increasing the residual silver concentration providing more Ag impurities placed next to low coordinated Au surface atoms. Recently, buried silver clusters have been reported[23]. Based on kinetic Monte-Carlo simulations it has been concluded that these clusters were a relict from the dealloying process but quantification is missing and a link to catalytic results is not provided.

To explain the role of silver in the catalytic activity of npAu, electron tomography based on energy dispersive X-ray spectroscopy (EDXS) is used in order to determine how the residual Ag is distributed quantitatively in the nanoporous structure. Furthermore, we complete the characterisation of the samples by a systematic study of ligament sizes and density of low coordinated surface atoms as a function of the residual silver concentration using transmission electron microscopy (TEM). Structural and chemical characterisations have been performed at nanoporous samples before the use as a catalyst.

2. Results and discussion

2.1. Catalytic oxidation of CO and methanol

Nanoporous gold was discovered to be an active catalyst for a variety of oxidation reactions such as the oxidation of CO, d-glucose, amines and primary alcohols such as methanol and ethanol[1–7]. While

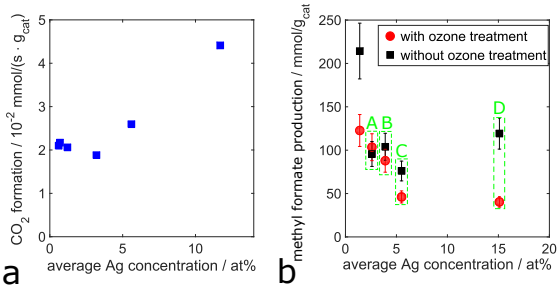

Figure 1: Oxidation reactions using O_2 over nanoporous gold catalysts with varying Ag content. (a) Gas phase catalytic oxidation of CO at 40 °C (10 vol% CO, 5 vol% O_2) in a plug flow reactor. (b) Aerobic oxidation of methanol to methyl formate at 60 °C and 3 bar O_2 in a stirred batch reactor (concentration of methyl formate referred to the amount of catalyst after 24 hours). Aliquots of the same sample (discs broken into several pieces) were investigated either as is (black squares) or after exposure to an ozone containing atmosphere (red circles). Average Ag concentration refers to average concentration in whole npAu disc measured by atomic absorption spectroscopy (AAS).

the use of molecular oxygen (O_2) is preferable instead of using much harsher chemicals such as hydrogen peroxide (H_2O_2), its activation and bonding on gold type surfaces is a controversial subject[26,27]. The presence of small amounts of the less noble and more reactive Ag inside the npAu host material renders its contribution highly likely. Samples prepared with different amounts of residual silver show distinctively different catalytic activity and conversion as shown in Fig. 1. It appears that for CO oxidation with O_2 a higher fraction of Ag is beneficial resulting in a higher catalytic activity (Fig. 1a) as also reported in previous studies[7]. While for samples with Ag contents of around 1 at% the activity is around 20 μmol/(s · g_{cat}), it is increased by more than 100 % for samples containing more than 10 at% of Ag. This trend could also

be observed for supported Au-Ag nanoparticle catalysts[16]. Simply, the increased fraction of Ag results in more active sites for the bonding and activation of O_2 which can react with CO adsorbed on either Au or Ag sites[24,25].

Noteworthy, a direct or linear correlation between the content of Ag and the catalytic activity cannot be drawn for the npAu catalysts. Samples with higher Ag content can also show inferior catalytic activity. As shown in Fig. 1b experiments on the aerobic oxidation of methanol in liquid phase using npAu catalysts show a strong influence of the Ag content on the conversion, here the concentration of the coupling product of methanol (methyl formate). Previous results from the gas phase catalytic oxidation of methanol already suggested that the presence of Ag may not only result in a higher activity by providing more reactive oxygen, but fosters total oxidation or build-up of inactive intermediates such as surface bonded formate[6]. Here, this trend can be confirmed also for the liquid phase oxidation reaction, where the formation of the coupling product is reduced by half when the average Ag content in the whole sample is increased from around 1 at% to 15 at%.

Recently, a pretreatment by ozone (O_3) was reported to result in an altered and enhanced catalytic performance for methanol oxidation in gas phase[28]. This was tested for the liquid phase oxidation by treating aliquots of one sample disc broken into several pieces either by ozone before measurement or using them in their pristine state. In general, the observed formation of the coupling product was reduced up to 30 % as compared to the pristine npAu (Fig. 1b). This treatment was demonstrated to result in the oxidation and removal of hydrocarbons from the surface[29], however, it also resulted in pronounced oxidation of the Ag[30]. The considerably lower temperatures required in liquid phase oxidation (below 80 °C as compared to more than 150 °C in gas phase) may explain why this pretreatment can result in such different behaviour. In order to understand the role of Ag and its oxidized states such as Ag_2O, more detailed information on its spatial distribution are clearly required.

2.2. Measurement of residual silver distribution

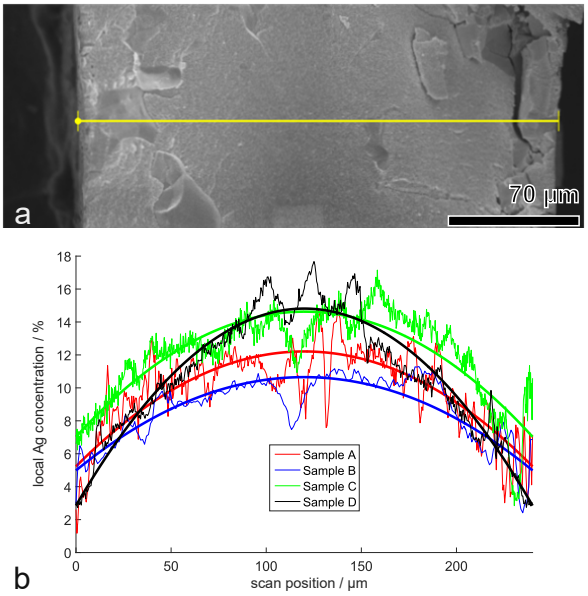

Figure 2: EDXS measurement of the silver distribution in a cross-section of a npAu disc. (a) SEM image showing exemplified a position where EDXS line scans were aquired. (b) comparison of the four samples labelled in Fig. 1. As a guide to the eye measurements are fitted by a parabola (thick lines). For all investigated samples the Ag concentration is higher in the center of the disc compared to the outer surface.

The average concentration of residual silver in the whole nanoporous gold sample after dealloying

as given in Fig. 1 has been determined using atomic absorption spectroscopy (AAS). With this method the total amount of silver in the npAu discs can be determined to prove that indeed samples with different residual Ag concentrations have been derived. Despite the high accuracy of this technique it only provides the total concentration of Ag in the entire sample but no information on its spatial distribution can be obtained. As shown by Hodge et al. strong concentrational gradients can exists on the scale of microns along the cross-section of a npAu disc[18]. For the four samples labelled in Fig. 1 as sample A, B, C and D a more detailed characterisation is shown in Fig. 2, where evaluations of EDXS line scans in cross-sections of cleaved npAu discs are depicted. These measurements have been carried out in a scanning electron microscope (SEM). All samples show an increased Ag concentration in the center of the disc compared to the outer surface. The reason for this increase can be explained by the fact that the silver from the center of the disc has a longer way to leave the sample compared to the silver close to the surface of the disc. A further comparison of the four samples reveals that although sample D shows the highest silver concentration in the center of the disc the concentration close to the outer surface of the disc is the lowest. The AAS measurements shown in Fig. 1 indicate increasing Ag content from sample A to sample D, whereas the EDXS line scans show increasing silver content in the order sample B, A, D, C. Summing up, the measurements show, that the Ag concentration in the npAu disc is varying strongly.

As the real chemical reactions occur at reactive atomic surface sites of the catalyst it is necessary

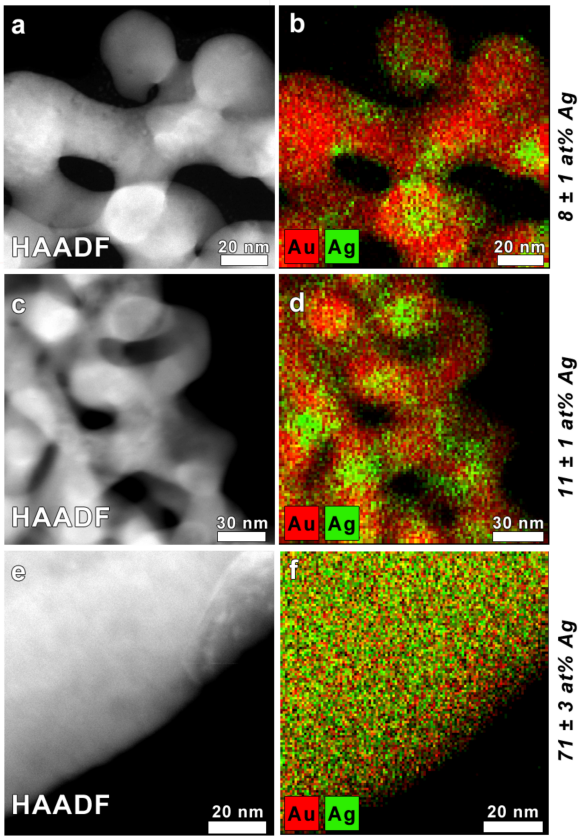

Figure 3: Elemental distribution of gold (red signal) and silver (green signal) for three samples with different residual Ag concentrations. For the nanoporous samples Ag cluster formation is clearly visible (b and d). These clusters cannot be seen in the parent alloy (f), indicating that clusters form during dealloying. Nanoporous sample with lower local average Ag concentration corresponds to sample B in Fig. 1, sample with higher local average Ag content corresponds to sample D.

to investigate the elemental distribution on smaller length scales. This characterization was achieved by means of scanning TEM (STEM) in combination with EDXS. For this purpose thin, electron transparent lamellas of npAu have been prepared using a standard focussed ion beam (FIB) lift out technique[31]. Fig. 3 shows representative measurements depicting the high-angle annular dark

field (HAADF) signal and the elemental distribution map for three different samples. Fig. 3b and d show maps of the porous structure of two different samples in regions with local average Ag concentrations of (8 ± 1) at% and (11 ± 1) at%, respectively, where local average Ag concentration refers to the average Ag concentration in the sample prepared for TEM. The sample with lower local average Ag concentration corresponds to sample B in Fig. 1, the sample with higher local average Ag content corresponds to sample D. Fig. 3f represents a sample prepared from the parent alloy before dealloying confirming the alloy concentration of (71 ± 3) at% Ag. Quantification has been done using the ζ-factor method [32] with ζ-factors determined by Zanaga et al. [33].

For the two nanoporous samples Fig. 3 shows that the silver (green signal) is not distributed homogeneously within the ligaments. Instead, silver rich clusters of different sizes can be observed. In regions between the clusters nearly no Ag signal is detected for the sample with the lower average Ag concentration, the sample with higher average concentration shows Ag signal also in regions between silver patches. To rule out the possibility of cluster formation caused by the FIB preparation of the samples or that the clusters are already existent in the parent alloy, elemental maps have been acquired at a FIB prepared sample from the $Au_{30}Ag_{70}$ parent alloy. A representative map is shown in the lower part of Fig. 3 showing that the elemental distribution is much more homogeneous in this case. This excludes that the Ag clusters are existent in the parent alloy and shows that they form during the dealloying process. Also the formation of clusters due to the preparation process can be excluded as all samples investigated here have been prepared in the same manner.

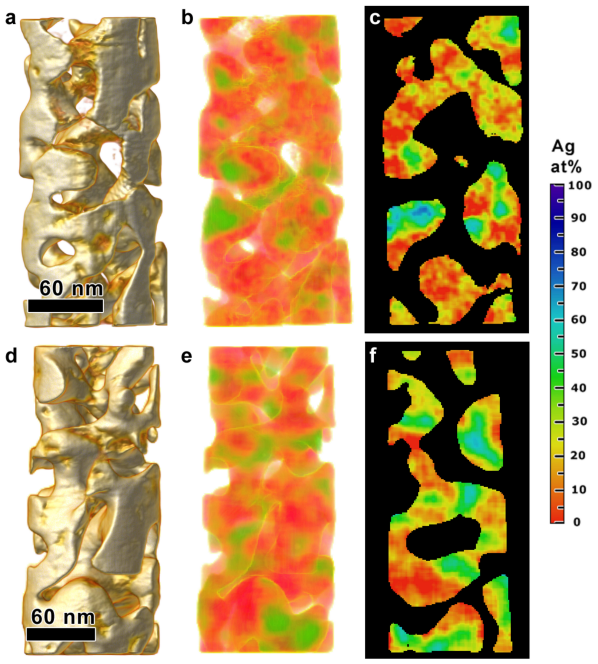

Figure 4: Tomographic reconstruction of the elemental distribution in nanoporous gold. (a),(d) reconstructions of the sample from HAADF signal, (b),(e) quantified elemental reconstructions, (c),(f) single slices of the reconstructed quantified elemental distributions. (a),(b),(c) average Ag concentration of about 8 at% (sample B), (d),(e),(f) local average Ag concentration of about 11 at% (sample D). Sample with lower local average Ag concentration shows higher Ag concentration in the Ag rich patches than samples with higher local average Ag concentration. The region between patches shows higher Ag concentrations for the sample with higher average Ag concentration. Silver enriched regions are distributed irregularly, both on the surface and inside the ligaments.

The results from the preceding paragraph partly confirm the assumption made earlier, for example by Haruta [19] who assumed small Ag_2O patches on the surfaces of the npAu ligaments. However, from two-dimensional projections the location of

Ag clusters in the 3D porous structure remains unclear. To answer this important question tomography experiments have been performed, acquiring the HAADF signal as well as the EDXS signal (for details see the methods section), quantified reconstructions of the elemental distribution were obtained using the approach proposed by Zanaga et al. [34]. In this manner the three-dimensional silver distribution in npAu samples of two different silver concentrations has been determined. The result is shown in Fig. 4, where Fig. 4a-c show results of a npAu sample with a local average silver concentration of (8 ± 1) at% and Fig. 4d-f represent a sample in a region with a local average silver concentration of about (11 ± 1) at%. The samples correspond to samples B and D in Fig. 1, respectively. The full reconstruction videos are provided in the supporting information.

Fig. 4a and d show renderings of the volume reconstruction using the HAADF signal, Fig. 4b and e show renderings of the quantified elemental reconstruction and Fig. 4c and f show single slices of the quantified elemental reconstruction. As these slices have a thickness of only 1.22 nm the quantitative silver distribution is spatially resolved with an accuracy better than 5 %. Firstly, it can be observed that the silver rich regions are located inside the ligaments, but also on the ligament surfaces. This excludes that the silver clusters are only buried relicts of the dealloying process representing parts of the material that have not been exposed to corrosion. Surprisingly, the silver concentration in the silver rich regions can possibly be even higher than in the parent alloy as can be seen for example in Fig. 4c where a blue region, indicating a silver concentration > 70 at% is visible. In silver depleted regions the silver concentration is higher for the sample with higher average silver concentration. This strengthens our former assumption concluded from the 2D elemental distribution that the formation of silver clusters occurs during dealloying.

In conclusion, our results provide important insights in the chemical composition of npAu as a result of the dealloying process, that also comply with hypothesis and studies reported in literature: Firstly, the silver is mainly located in patches or clusters, secondly, the clusters can be located either inside the ligaments or on the surfaces and finally, the formation of silver clusters is a process that occurs during dealloying leading to Ag concentrations in the clusters that can possibly be locally higher than in the parent alloy.

2.3. Structural properties

The variation of ligament sizes with residual silver concentration has been reported [4,18,23], showing that ligaments with high silver concentration are smaller than ligaments with low silver content. However, the results suffer from the subjective nature of a manual measurement. Furthermore, as shown in the preceding section the silver concentration in a cross-section of a npAu disc is not homogeneous. Hence also the size distribution is not homogeneous and depends on the region at which the images are obtained. An alternative approach for the comparison of size distributions in npAu is proposed by Fujita and Chen [35]. The dealloying process of the gold-silver alloy can be described as a process of spinodal decomposition [36]. In this case decomposition means a separation between *mate-*

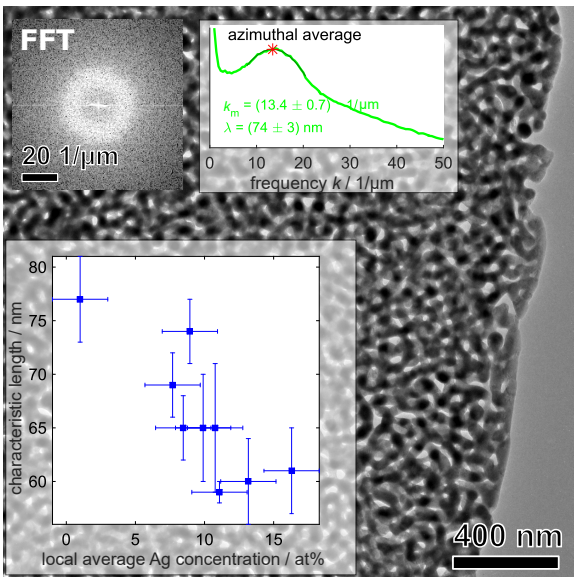

Figure 5: Characteristic length as a function of the residual silver concentration. The power spectrum of the Fourier transform (upper left inset) of a low magnification TEM image (background) is averaged azimuthally (upper right inset) and the maximum giving the characteristic length is determined by a parabola fit. The characteristic length describing the average separation between centres of neighbouring ligaments is decreasing with increasing residual silver concentration. Ag concentration measured by EDXS gives local average concentration for each TEM sample.

rial and *no material*. According to theoretical descriptions of spinodal decomposition[37,38] a characteristic peak comes up in the Fourier transform of a map after decomposition, in the case of npAu this is a map which distinguishes between material (ligament) and no material (pore). In this way Fujita and Chen took low magnification images of npAu in a TEM, calculated the power spectra of their Fourier transforms and averaged them azimuthally. In these averages a clear peak is visible describing the characteristic length of the npAu sample, which gives the averaged separation between centres of neighbouring ligaments. A further advantage of this method is that a corresponding EDXS spectrum can be obtained for each small TEM sample giving a more accurate local average silver concentration. Fig. 5 shows the characteristic length of npAu as a function of the residual silver concentration measured by EDXS. Although there are deviations a clear trend is visible, confirming that the more residual silver is in the sample the smaller is the separation between centres of neighbouring ligaments and hence ligaments and pores are smaller.

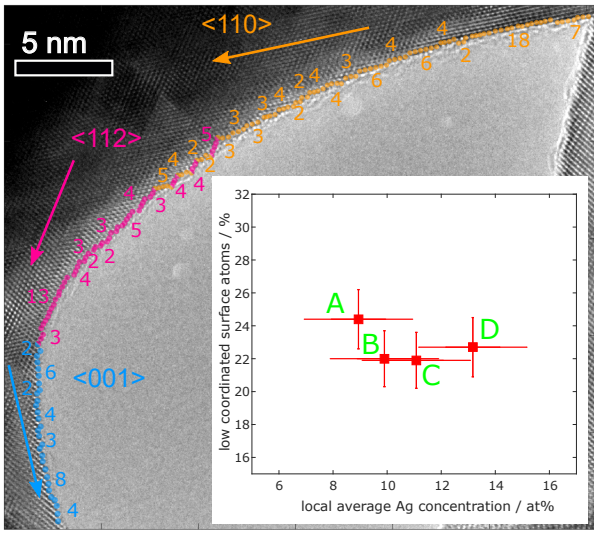

Figure 6: Percentage of low coordinated surface atoms as a function of the residual silver concentration. Distances between surface steps are measured for different crystallographic orientations separately (background), averages are calculated and weighted with reciprocal free surface energies to obtain the percentage of low coordinated surface atoms. No relationship between percentage of low coordinated surface atoms and residual silver concentration can be found. Ag concentration measured by EDXS gives local average concentration for each TEM sample.

Besides the chemical composition, the catalytic activity of npAu is based on the density of low coordinated surface atoms[39]. For a determination

of this density in principle a 3D atomic reconstruction of the ligaments would be necessary, but due to the size of the structure, an atomic reconstruction would be extremely challenging. An approximation is proposed by Fujita et al., who measured separations between atomic surface steps in two-dimensional projections of the sample[40]. Averages have been calculated for each crystallographic direction separately whereas no distinction between $< 112 >$ and $< 11\bar{2} >$ directions has been made as both correspond to [111]-like surfaces. As surfaces with high surface energies are less favourable than surfaces with low surface energies averages have been calculated for each surface separately. Subsequently, these averages have been weighted with reciprocal surface energies[41] to account for the frequency of existence for each surface. In this manner an approximation for the density of low coordinated surface atoms can be obtained as a function of the local average silver concentration as depicted in Fig. 6. No clear relationship can be found, in all cases around 22 % of the surface atoms are low coordinated which is close to values that can be found for nanoparticles[40]. It should be noted that especially for samples with higher Ag concentrations it is sometimes difficult to find npAu surfaces with a clearly visible crystal structure. A higher silver concentration means a higher probability of finding silver also on the surface of a ligament. In this case it is possible that Ag forms oxides, which do not necessarily have a face centered cubic crystal structure[42] as for gold, silver or its alloy. This is an additional hint that residual silver is not only buried inside ligaments but that it is also located on the surface.

2.4. Discussion

The role of residual silver in the catalytic activity of nanoporous gold is ambiguous. Our results show highest yield of methyl formate for the oxidation of methanol in presence of the lowest residual silver concentration. This is in agreement with the results from the gas phase, but stays in contrast to the oxidation of CO or d-glucose[4], both improving with higher residual Ag concentration. The reason for this discrepancy can be explained as follows: the fact that the CO_2 yield in CO oxidation increases with increasing residual silver concentration is hindering in the oxidation of methanol. As CO_2 production is supported by larger Ag content this is also the case in methanol oxidation suppressing the yield of the desired oxidation product methyl formate. Furthermore, a build-up of inactive intermediates such as surface bonded formate could be supported by more residual silver as reported in literature[6] for the gas phase oxidation of methanol. Therefore, our result confirms that whether the nanoporous gold catalyst should have more or less residual silver depends on the reactant to be oxidized. For the oxidation of methanol to methyl formate more residual silver is not beneficial, both in the liquid as well as in the gas phase. For this reaction longer dealloying times of the alloys are required to obtain npAu samples with the lowest possible residual silver concentration.

Our measurements concerning the spatial distribution of the residual silver answer an important question, but they also give rise to new ones: the gradient in the silver concentration from the surface of the npAu disc towards its center in cross-sections of the discs leads to the question of the real Ag con-

centration in that part of the sample that can take part in a catalytic process. Although depending on the pore size, it is obvious that not all reactants succeed in reaching the center of the nanoporous disc. For pore sizes of $\approx 40\,\mathrm{nm}$ nearly no reactant reaches a depth of $50\,\mu\mathrm{m}$ according to a diffusion model described by Wittstock et al. [17]. The EDXS line scans in Fig. 2 reveal the lowest Ag concentration close to the surface of the npAu disc for the sample with the highest average Ag concentration (sample D). The catalytic activity of this sample shown in Fig. 1 is better than that of samples A-C, opposing the general trend, indicating that the catalytic activity is basically controlled by the lower Ag concentration close to the surface of the npAu disc. This leads to two basic conclusions: firstly, Ag has a strong influence on the catalytic activity and secondly, giving only one average Ag concentration for a whole npAu disc is only a rough approximation, because the local composition is varying strongly. To reach nanoporous gold with a more homogeneous silver distribution different sample geometries or further treatment of the samples such as crushing would be necessary. Also for catalytic reactions that benefit from larger silver concentrations further treatment of the samples would be advantageous. In this way the inner part of the npAu disc with higher silver concentration could take part in the catalytic reaction more efficiently.

We found that the formation of silver rich clusters is more pronounced the less silver remains in the sample. In samples with large silver content the silver distribution is more homogeneous, because especially in regions in between the clusters the silver concentration is increased. This emphasizes the fact that the spatial distribution of the Ag plays a key role in the catalytic process. For oxidation reactions that are promoted by residual silver an homogeneous distribution of Ag, rather than the presence of clusters with high Ag concentration seems to be beneficial. Although the residual silver concentration of less than 1 at% in completely dealloyed samples is too low to be spatially resolved the results shown here give rise to the assumption that the residual silver in these samples could also be located in form of clusters as the less silver is present the more pronounced the cluster formation is visible. Although this is only an assumption, in this manner for samples with low silver content and hence strong cluster formation the interface between silver rich and silver depleted regions would play the key role in the catalytic reaction as in these regions atoms of different types would be located more frequently next to each other supporting the adsorption of different reactants.

The presence of subsurface Ag also in the form of agglomerates and clusters in the npAu was reported recently [23]. So far, these agglomerates were discussed to originate during corrosion of the material by which Ag atoms are trapped inside the Au ligaments. This also led to the contradiction that the catalysis of the material cannot be affected by Ag as it is not located at the surface. Of course, bimetallic surfaces, in particular under reactive conditions, even when exposed to the ambient air and oxygen, are not static but subject to change. Nevertheless, here we can clearly show that Ag is present at the surface and has a strong impact on the catalytic activity of the material.

3. Conclusions

The quantitative distribution of residual silver in nanoporous gold has been determined, partially verifying different assumptions made in the literature. Silver forms clusters that evolve during dealloying of a gold-silver alloy. Cluster formation is more pronounced if less residual silver remains in the sample. Silver clusters are observed inside the material as well as on the surface. The less residual silver remains in the porous structure, the larger pores and ligaments get. The density of low coordinate surface atoms is constant within the margins of error, being independent of the residual silver concentration. Nanoporous gold discs are dealloyed inhomogeneously, leaving more residual silver in the center of the discs compared to their surfaces. Whether silver is beneficial for the catalytic performance of npAu depends basically on the reaction to be promoted. For the oxidation of methanol to methyl formate more residual silver is disadvantageous whereas oxidation of CO is supported by more residual silver in the liquid as well as in the gas phase.

4. Methods

4.1. Sample preparation

Nanoporous gold samples (npAu) were prepared from $Au_{30}Ag_{70}$ master alloys in the form of discs (5 mm in diameter, 0.25 mm in thickness, subscript numbers indicate atomic percent). Samples with low residual Ag content (i.e. < 1 at%) were prepared by galvanic, also dubbed 'free' corrosion (see also Ref.[17]). In this case the sample was submersed in concentrated nitric acid (HNO_3, Sigma-Aldrich, > 65 weight%) at room temperature for 24 hours, followed by careful removal and replacement of the acid by deionized water for at least three times. Samples were dried in air for at least 24 hours. Samples with elevated residual Ag concentration were prepared by potentiostatic corrosion using a typical three electrode setup (Potentiostat BioLogic SP200). Typically a gold wire formed as a basket and holding the alloy was used as the working electrode, as well as a platinum counter electrode and a platinum quasi reference electrode. The etching process occurred at 60 mV with dipped electrodes in 5M nitric acid (HNO_3, Sigma-Aldrich, > 65 weight%) at room temperature (see also Ref.[6]). An alternative technique using perchloric acid[43] was employed for one sample (cf. Fig. 1a, sample with 3.2 at% residual Ag). In this case a 1M solution of perchloric acid (Sigma Aldrich, 70 % and high purity water, $> 18\,M\Omega$) was used as an electrolyte and a Ag/AgCl (3 M KCl) reference electrode (separated from the compartment by a Haber-Luggin capillary) was used. In all cases, the potential was applied till desired amount of Ag was removed according to Eq. 1, where c_{Ag} gives the residual silver concentration (atom %), $q(t)$ is the electrochemical charge (one electron corresponding to one Ag atom removed/oxidized), m_{alloy} denotes the mass of the alloy, w_{Ag} the Ag concentration in the parent alloy (weight %), $F = 96485 \frac{C}{mol}$ is the Faraday constant and M_{Ag} is the molar mass of Ag.

$$c_{Ag} = \frac{q(t)}{F \cdot m_{alloy} \cdot \frac{w_{Ag}}{M_{Ag}}} \quad (1)$$

For the pretreatment of samples using ozone (O_2,

Linde 5.0 feed), an ozone generator (Type 802 N, BMT Messtechnik Berlin) and an ozone analyser (Type 964, BMT Messtechnik Berlin) were used. Samples were placed in a glass compartment and a stream of ozone containing atmosphere (typical $\approx 5-10\%$) was introduced for at least 3 hours.

4.2. Catalysis

Gas phase oxidation of CO was performed using a setup described in previous publications[17]. The reactor was entirely made of glass (inner diameter 20 mm, total volume of 26 mL) and the sample placed on a gold plate (2 g) at the reactor entrance. As heating of the catalyst sample by the strongly exothermic CO oxidation can have a noticeable impact on the measurement, the gold plate (mass > 100 times more than the catalyst samples) was used as a heat sink. The temperature of the reactor was controlled by liquid heating and cooling. The feed consisted of a mixture of CO (Linde AG, 4.7), N_2 (Linde, 5.0), and O_2 (Linde, 5.0). The total flow was set to 50 sccm or ml/min and controlled via mass flow controllers (Maettig Bronkhorst, Netherlands).

Liquid phase oxidation reactions were carried out in a reactor (AmAr Equipments PVT.LTD.). Temperature of liquid phase and pressure of gas phase above liquid phase were controlled by installed thermocouple and pressure gauges. The reactor was filled with 60 mL of methanol (MeOH, VWR Chemicals, 100 %). To avoid mechanical damage during catalysis the npAu catalyst was mounted in a metallic net basket inside the reactor. After sealing of the reactor, the liquid phase was continuously stirred and cooled by water line, purged with nitrogen and oxygen each twice, pressurized with oxygen pressure and heated to 60 °C for 24 hours. The obtained self-coupling product methyl format was determined quantitatively via Gas Chromatography coupled with a mass spectrometer (GC/MS, Agilent Technologies, 5975C, inert XL MSD, with Triple-Axis Detector), equipped with an Agilent CS column (50 m x 250 μm x 0.1 μm). Commercial chemical of methyl formate (Alfa Aesar, 97 %) was used as external standard to assign GC peaks and its detectability limitation was 0.03 mmol.

4.3. Characterisation

Measurement of the averaged silver concentration in the npAu discs has been performed using atomic absorption spectroscopy on a Analytic Jena FL5. Energy dispersive X-ray measurements on the SEM have been performed on a FEI Helios NanoLab 600 SEM equipped with a Oxford X-Max 80 EDX detector (125eV energy resolution for Mn K_α) using an acceleration voltage of 20 kV.

Sample preparation for the TEM has been done with a focussed ion beam (FIB) using a standard lift-out technique[31] on a FEI Nova 200 FIB in Bremen, with an acceleration voltage of 30 kV and a beam current of 50 pA for the final milling step. For the tomography experiments circular shaped needles with diameters of ≈ 120 nm have been prepared in Antwerp with a FEI Helios NanoLab 650 using an acceleration voltage of 30 kV and a beam current of 7.7 pA for the final milling step.

TEM measurements for the characteristic length of npAu, density of low coordinated surface sites and local average Ag concentrations in the TEM lamellas have been carried out in Bremen using a

FEI Titan 80/300 TEM/STEM equipped with an EDAX spectrometer (TOPS 30 OST 1365) and an aberration corrector for the imaging system operated at 300 kV. Two-dimensional elemental distribution mapping and tomography experiments have been performed in Antwerp using a FEI Tecnai Osiris equipped with Schottky FEI X-FEG and a ChemiSTEM system, operated at an acceleration voltage of 200 kV. For the STEM tomography measurements a tilt series from $-78\,^\circ$ to $+78\,^\circ$ with steps of $2\,^\circ$ and a frame time of 10 s has been acquired, for the EDXS tomography steps of $10\,^\circ$, a frame time of 400 s and a screen current of approximately 200 pA have been used. Measurements have been carried out using a 2050 Fischione Instruments tomography holder. The EDXS tomography reconstructions were obtained using the approach proposed by Zanaga et al. [34].

Acknowledgements

This work was supported by the Deutsche Forschungsgemeinschaft (DFG) under contracts no. RO2057/12-1 (SP 6) and WI4497/1-1 (SP 2) within the research unit FOR2213 (`www.nagocat.de`) and the European Research Council (ERC Starting Grant No. 335078-COLOURATOMS).

Supporting Information

- auag8_movie.mpg: 3D tomographic reconstruction video of a nanoporous gold sample in a region with a local average Ag concentration of 8 at%.
- auag11_movie.mpg: 3D tomographic reconstruction video of a nanoporous gold sample in a region with a local average Ag concentration of 11 at%.

References

[1] Zielasek, V.; Jürgens, B.; Schulz, C.; Biener, J.; Biener, M. M.; Hamza, A. V.; Bäumer, M. *Angewandte Chemie International Edition* **2006**, *45*, 8241–8244.

[2] Zhang, J.; Liu, P.; Ma, H.; Ding, Y. *The Journal of Physical Chemistry C* **2007**, *111*, 10382–10388.

[3] Xu, C.; Su, J.; Xu, X.; Liu, P.; Zhao, H.; Tian, F.; Ding, Y. *Journal of the American Chemical Society* **2007**, *129*, 42–43, PMID: 17199279.

[4] Yin, H.; Zhou, C.; Xu, C.; Liu, P.; Xu, X.; Ding, Y. *The Journal of Physical Chemistry C* **2008**, *112*, 9673–9678.

[5] Ding, Y.; Chen, M. *MRS bulletin* **2009**, *34*, 569–576.

[6] Wittstock, A.; Zielasek, V.; Biener, J.; Friend, C. M.; Bäumer, M. *Science* **2010**, *327*, 319–322.

[7] Wittstock, A.; Biener, J.; Bäumer, M. *Phys. Chem. Chem. Phys.* **2010**, *12*, 12919–12930.

[8] Kramer, D.; Viswanath, R. N.; Weissmüller, J. *Nano Letters* **2004**, *4*, 793–796.

[9] Detsi, E.; Chen, Z.; Vellinga, W.; Onck, P.; De Hosson, J. *Journal of nanoscience and nanotechnology* **2012**, *12*, 4951–4955.

[10] Zeis, R.; Lei, T.; Sieradzki, K.; Snyder, J.; Erlebacher, J. *Journal of Catalysis* **2008**, *253*, 132 – 138.

[11] Pickering, H. W.; Swann, P. R. *Corrosion* **1963**, *19*, 373t–389t.

[12] Forty, A. J. *Nature* **1979**, *282*, 597–598.

[13] Erlebacher, J. *Journal of the Electrochemical Society* **2004**, *151*, C614–C626.

[14] Iizuka, Y.; Kawamoto, A.; Akita, K.; Daté, M.; Tsubota, S.; Okumura, M.; Haruta, M. *Catalysis Letters* **2004**, *97*, 203–208.

[15] Wang, A.-Q.; Liu, J.-H.; Lin, S.; Lin, T.-S.; Mou, C.-Y. *Journal of Catalysis* **2005**, *233*, 186 – 197.

[16] Jürgens, B.; Kübel, C.; Schulz, C.; Nowitzki, T.; Zielasek, V.; Biener, J.; Biener, M. M.; Hamza, A. V.; Bäumer, M. *Gold Bulletin* **2007**, *40*, 142–149.

[17] Wittstock, A.; Neumann, B.; Schaefer, A.; Dumbuya, K.; Kübel, C.; Biener, M. M.; Zielasek, V.; Stein-

rück, H.-P.; Gottfried, J. M.; Biener, J.; Hamza, A.; Bäumer, M. *The Journal of Physical Chemistry C* **2009**, *113*, 5593–5600.

[18] Hodge, A.; Doucette, R.; Biener, M.; Biener, J.; Cervantes, O.; Hamza, A. *Journal of Materials Research* **2009**, *24*, 1600–1606.

[19] Haruta, M. *ChemPhysChem* **2007**, *8*, 1911–1913.

[20] Wittstock, A.; Wichmann, A.; Bäumer, M. *ACS Catalysis* **2012**, *2*, 2199–2215.

[21] Ide, M. S.; Davis, R. J. *Accounts of Chemical Research* **2014**, *47*, 825–833, PMID: 24261465.

[22] Wittstock, A.; Bäumer, M. *Accounts of Chemical Research* **2014**, *47*, 731–739, PMID: 24266888.

[23] Krekeler, T.; Straßer, A. V.; Graf, M.; Wang, K.; Hartig, C.; Ritter, M.; Weißmüller, J. *Materials Research Letters* **2017**, *0*, 1–8.

[24] Moskaleva, L. V.; Rohe, S.; Wittstock, A.; Zielasek, V.; Klüner, T.; Neyman, K. M.; Bäumer, M. *Phys. Chem. Chem. Phys.* **2011**, *13*, 4529–4539.

[25] Moskaleva, L. V.; Zielasek, V.; Klüner, T.; Neyman, K. M.; Bäumer, M. *Chemical Physics Letters* **2012**, *525 - 526*, 87 – 91.

[26] Gottfried, J.; Schmidt, K.; Schroeder, S.; Christmann, K. *Surface Science* **2003**, *525*, 184 – 196.

[27] Green, I. X.; Tang, W.; Neurock, M.; Yates, J. T. *Science* **2011**, *333*, 736–739.

[28] Personick, M. L.; Zugic, B.; Biener, M. M.; Biener, J.; Madix, R. J.; Friend, C. M. *ACS Catalysis* **2015**, *5*, 4237–4241.

[29] Stowers, K.; Madix, R.; Friend, C. *Journal of Catalysis* **2013**, *308*, 131 – 141, 50th Anniversary Special Issue.

[30] Schäfer, A.; Ragazzon, D.; Wittstock, A.; Walle, L. E.; Borg, A.; Bäumer, M.; Sandell, A. *The Journal of Physical Chemistry C* **2012**, *116*, 4564–4571.

[31] Giannuzzi, L.; Stevie, F. *Micron* **1999**, *30*, 197 – 204.

[32] Watanabe, M.; Williams, D. B. *Journal of Microscopy* **2006**, *221*, 89–109.

[33] Zanaga, D.; Altantzis, T.; Sanctorum, J.; Freitag, B.; Bals, S. *Ultramicroscopy* **2016**, *164*, 11 – 16.

[34] Zanaga, D.; Altantzis, T.; Polavarapu, L.; Liz-Marzán, L. M.; Freitag, B.; Bals, S. *Particle & Particle Systems Characterization* **2016**, *33*, 396–403.

[35] Fujita, T.; Chen, M. W. *Japanese Journal of Applied Physics* **2008**, *47*, 1161.

[36] Erlebacher, J.; Aziz, M. J.; Karma, A.; Dimitrov, N.; Sieradzki, K. *Nature* **2001**, *410*, 450–453.

[37] Cahn, J. W. *The Journal of Chemical Physics* **1965**, *42*, 93–99.

[38] Berk, N. F. *Phys. Rev. Lett.* **1987**, *58*, 2718–2721.

[39] Lopez, N.; Janssens, T.; Clausen, B.; Xu, Y.; Mavrikakis, M.; Bligaard, T.; Nörskov, J. *Journal of Catalysis* **2004**, *223*, 232 – 235.

[40] Fujita, T.; Guan, P.; McKenna, K.; Lang, X.; Hirata, A.; Zhang, L.; Tokunaga, T.; Arai, S.; Yamamoto, Y.; Tanaka, N.; Ishikawa, Y.; Asao, N.; Yamamoto, Y.; Erlebacher, J.; Chen, M. *Nat Mater* **2012**, *11*, 775–780.

[41] Singh-Miller, N. E.; Marzari, N. *Phys. Rev. B* **2009**, *80*, 235407.

[42] Pearson, W.; Villars, P.; Calvert, L. *Pearson's Handbook of Crystallographic Data for Intermetallic Phases*; Pearson's Handbook of Crystallographic Data for Intermetallic Phases Bd. 2; American Society for Metals, 1985; pp 868.

[43] Cattarin, S.; Kramer, D.; Lui, A.; Musiani, M. M. *The Journal of Physical Chemistry C* **2007**, *111*, 12643–12649.